https://doi.org/10.5194/egusphere-2023-1016
Preprint. Discussion started: 14 June 2023

Low Temperature Ice Nucleation of Sea Spray and Secondary Marine Aerosols under Cirrus Cloud Conditions

Ryan J. Patnaude[1], Kathryn A. Moore[1], Russell J. Perkins[1], Thomas C. J. Hill[1], Paul J. DeMott[1], and Sonia M. Kreidenweis[1]

[1]Department of Atmospheric Science, Colorado State University, Fort Collins, 80521, USA

Correspondence to: Ryan Patnaude (ryan.patnaude@colostate.edu)

Abstract. Sea spray aerosols (SSA) represent one of the most abundant aerosol types on a global scale and have been observed at all altitudes including the upper troposphere. SSA has been explored in recent years as a source of ice nucleating particles (INPs) in cirrus clouds due to the ubiquity of cirrus clouds and the uncertainties in their radiative forcing. This study expands upon previous works on low temperature ice nucleation of SSA by investigating the effects of atmospheric aging of SSA and the ice nucleating activity of newly formed secondary marine aerosols (SMA) using an oxidation flow reactor. Polydisperse aerosol distributions were generated from a Marine Aerosol Reference Tank (MART) filled with 120 L of real or artificial seawater and their subsequent freezing was measured using a Continuous Flow Diffusion Chamber (CFDC). Results show that for both primary SSA (pSSA), and the aged SSA and SMA (aSSA+SMA) at temperatures > 220 K, 1 % of the particles freeze via homogeneous nucleation. However, below 220 K, heterogeneous nucleation occurs for both pSSA and aSSA+SMA at much lower relative humidities (RHs), where up to 1 % of the aerosol population freezes between 75–80 % RH. Similarities between freezing behaviors of the pSSA and aSSA+SMA at all temperatures suggest atmospheric aging has little effect on the heterogeneous freezing behavior of SSA at these cirrus temperatures and remains dominated by the crystalline salts. Occurrence of 1 % frozen fraction of SMA, generated in the absence of primary SSA, was observed at/near water saturation below 220 K, suggesting it is not an effective INP at cirrus temperatures, similar to findings in the literature of other organic aerosols. Thus, any SMA coatings on the pSSA are also unlikely to modify the ice nucleation behavior of pSSA. These results demonstrate the ability of lofted primary sea spray particles to remain an effective ice nucleator at cirrus temperatures, even after atmospheric aging.

1. Introduction

Cirrus clouds are present at temperatures below 235 K and are composed entirely of ice. With widespread global coverage, cirrus clouds have a significant effect on the Earth's radiation budget (Baker, 1997; Chen et al., 2000; Liou, 1986; Sassen et al., 2008; Wylie et al., 1994). The sign of the radiative effect of cirrus clouds is controlled by their microphysical properties (Jensen et al., 1994; Schumann et al., 2012; Zhang et al., 1999), which are directly affected by the formation pathway. Ice nucleation in cirrus clouds at temperatures < 235 K can proceed via two basic processes, homogeneous or heterogeneous nucleation. The homogeneous (or spontaneous) nucleation pathway is the process in which condensed water containing dissolved solute particles freezes at sufficiently high supersaturations and low enough temperatures (DeMott et al., 2003; Koop et al., 2000), while heterogeneous nucleation is controlled by the presence of ice nucleating particles (INPs), which lower the energy barrier required for the activation of a critical ice embryo (Hoose and Möhler, 2012; Vali et al., 2015). These two pathways will ultimately compete depending on the relative humidity (RH) and temperature conditions, which are driven by vertical motions (Kärcher et al., 2022), and the INP concentrations, which will define the lower RH threshold required for the onset of heterogeneous freezing. Homogeneous nucleation represents the upper bound RH for freezing and will depend upon the water activity of the dilute aerosol solutions and

https://doi.org/10.5194/egusphere-2023-1016
Preprint. Discussion started: 14 June 2023

temperature (Schneider et al., 2021). Homogeneous nucleation occurs at higher ice supersaturations (SS_i, relative humidity with respect to ice (RH_i) minus 100 %) than heterogeneous nucleation. Heterogeneous nucleation may follow a number of different freezing pathways depending on the temperature, RH, and aerosol composition. The immersion freezing mechanism occurs when an INP initiates freezing from within a sufficiently dilute aqueous solution droplet below water saturation or in a fully activated cloud condensation nucleus (CCN) under water supersaturated conditions (RH with respect to water, $RH_w > 100$ %). Deposition nucleation occurs at RHs between ice and water saturation, where water vapor initiates freezing directly onto an INP. However, in recent years this mechanism has been debated and some consider the freezing event to be a result of pore condensation freezing (PCF), where water vapor condenses into pores or cracks on the surface of an INP (David et al., 2019; Marcolli, 2014).

A wide range of aerosol types may act as INPs in cirrus clouds. Global airborne observations of cirrus cloud residual particles found that mineral dust and metallic particles made up the highest fraction of cirrus ice residuals (IRs) (Cziczo et al., 2004; Cziczo et al., 2013; Cziczo & Froyd, 2014). Laboratory studies using continuous flow diffusion chambers (CFDCs) have confirmed these observations, indicating that mineral dust and metal oxides may freeze via the immersion or deposition nucleation mode between -40 ºC and -60 ºC depending on the relative humidity and particle surface area (Archuleta et al., 2005; DeMott et al., 2003; Kanji & Abbatt, 2010). While black carbon and secondary organic aerosols (SOA) are found in abundance in the upper troposphere (Froyd et al., 2010; Schill et al., 2020; Schwarz et al., 2017) and appear to dominate IRs in cirrus contrails (Petzold et al., 1998), there is disagreement in their overall contributions as cirrus cloud INPs. Ammonium sulfate is abundant in the atmosphere and may also act in solid form as a cirrus INP, however, most studies have shown sulfate to freeze via heterogeneous nucleation at fractions too low to be meaningful compared to other INP types (Abbatt et al., 2006; Baustian et al., 2010; Wise et al., 2010). Sea salt particles, on the other hand, have been shown to make up a relatively large fraction, up to ~25 %, of the IRs in cirrus clouds, especially when collected over the ocean (Cziczo et al., 2013). Sea spray aerosols (SSA) are abundant in the atmosphere (Vignati et al., 2010) and may be lofted from the marine boundary layer to the upper troposphere via deep convection and detrainment from cirrus anvils, where they are available for subsequent cirrus ice nucleation.

Marine aerosols are generally separated into primary SSA and secondary marine aerosols (SMA). Primary SSA are produced by wind stress on the ocean surface, which causes wave breaking and the production of bubble-bursting film and jet drops, comprised of inorganic sea-salt and organic matter (O'Dowd and De Leeuw, 2007). SMA, on the other hand, may be produced via gas-to-particle conversion of the gas phase species that are emitted from the ocean, which includes dimethyl sulfide (DMS), a biproduct of marine phytoplankton, and other volatile organic compounds (VOCs) (Fitzgerald, 1991; O'Dowd and De Leeuw, 2007). DMS and VOCs may also alter the composition of primary SSA via condensation onto existing particles. SMA have been shown to be comprised primarily of non-sea-salt (nSS) sulfates and other secondary organic species, produced primarily from the oxidation of DMS, which can dominate the total submicron aerosol mass. (Fitzgerald, 1991; O'Dowd et al., 2004), However, observations in the North Atlantic showed wide variability in the submicron organic mass depending on season (Saliba et al., 2020). SMA may play an important role in cloud formation in oceanic regions, specifically by modulating the CCN concentrations. CCN concentrations in marine environments have been found to be directly related to DMS emissions (Berresheim et al., 1993; Pandis et al., 1994). Ship based measurements in the Southern Ocean found higher concentrations of CCN containing more biogenic sulfates and organics closer to Antarctica, where there is a greater source of biogenic emissions during austral summer (Sanchez et al., 2021). More recently, laboratory studies have focused on the impact of ocean emissions on atmospheric chemistry (Mayer et al., 2020a; Prather et al., 2013) and have utilized oxidation flow reactors (OFRs) (Peng and Jimenez, 2020) to study the formation of SMA and the aging processes of the primary SSA. For example, Mayer et al., (2020b) found that SMA generated from natural seawater using an OFR plays a dominant role in the formation of cloud droplets, compared to primary SSA. Despite the attention

https://doi.org/10.5194/egusphere-2023-1016
Preprint. Discussion started: 14 June 2023

given to studying the impact of SMA on CCN concentrations and the formation of liquid clouds, the ability of SMA to take part in ice nucleation in cirrus clouds is not well understood.

In contrast to SMA, the ice nucleating ability of primary SSA at cirrus temperatures has received more attention in recent years. A number of laboratory studies have observed heterogeneous nucleation behavior of NaCl, synthetic sea-salt, and SSA generated from real seawater at temperatures < 235 K (Schill & Tolbert, 2014; Wagner et al., 2018; Wagner & Möhler, 2013; Wise et al., 2012). Most significantly, the inorganic components of SSA have been found to freeze heterogeneously at high fractions (~10 %) below 225 K (Patnaude et al., 2021; Wagner et al., 2021), high enough to potentially compete with more conventionally effective INPs (i.e., mineral dust). While the non-sea-salt (nSS) components of primary SSA have been shown to act as heterogeneous INPs in the mixed-phase regime ($\gtrsim$ 235 K, presence of liquid and ice) (Ickes et al., 2020; McCluskey et al., 2018a), until recently less was known regarding the freezing of nSS components at cirrus temperatures. Possible types of primary marine organics may include bacteria, fatty acids, proteins, and saccharides (Wolf et al., 2019). A few recent studies have investigated the ice nucleating behavior of organic material at cirrus temperatures and found particles with a higher organic carbon fraction were more likely to freeze via heterogeneous nucleation below 235 K (Wagner et al., 2021; Wolf et al., 2019, 2020b). These studies illustrate the potential of the organic material and inorganic salts in seawater to initiate heterogeneous nucleation at cirrus temperatures. However, the pathway of SSA from the marine boundary layer to the upper troposphere where cirrus clouds reside would likely modify both the inorganic and organic components of these aerosols due to atmospheric oxidation. The question of whether atmospheric oxidation alters the ice nucleating ability of SSA at cirrus temperatures remains unanswered.

In this study, expanding upon the work in Patnaude et al., (2021), the low temperature ice nucleating ability of SSA, generated using a Marine Aerosol Reference Tank (MART) to resemble realistic ocean–atmosphere emissions, is investigated. Using an OFR, we examined the impact of atmospheric oxidation on freezing behavior of primary SSA at cirrus temperatures. In addition, the low temperature freezing behavior of SMA produced from gas-phase emission of seawater was investigated. Finally, we compared primary SSA and SMA generated from real seawater and an artificial seawater product to infer the roles of the organic material and inorganic sea salts on heterogeneous ice nucleation at cirrus temperatures.

2 Methods

A general overview of the experimental setup is shown in Figure 1. The following sections provide descriptions of each component of the aerosol generation and processing instrumentation and the design of the experiments.

2.1 Seawater collection and preparation

For this study, a Marine Aerosol Reference Tank (MART), originally developed by the NSF Center for Aerosol Impacts on Chemistry of the Environment (CAICE, Prather et al., (2013)), was used for generation of an atmospherically relevant size distribution of SSA by mimicking wave breaking in the ocean (Mayer et al., 2020; Stokes et al., 2013). The MART was filled with 120 L of 1) natural seawater (SW) collected at the Scripps pier in La Jolla, CA, 2) Neomarine (Brightwell Aquatics), a commercially available artificial seawater (ASW) product (3.5 % by weight) or 3) deionized water (DI). The ASW was mixed outside of the MART in 5-gallon plastic (LDPE/LLDPE) cubitainers, filtered through a TOC+HEPA filter and into the MART, then recirculated through the filter using a peristaltic pump for ~24 hours to remove residual organic carbon. The seawater was shipped overnight at room temperature to Colorado State University in the same cubitainers, which had been acid washed prior to use in mixing the ASW, then thoroughly rinsed with deionized water before SW collection. During seawater collection, the water was filtered through a 50-µm food-grade woven polyester mesh, which was pre-cleaned with methanol and 5 % hydrogen peroxide and rinsed

https://doi.org/10.5194/egusphere-2023-1016
Preprint. Discussion started: 14 June 2023

with deionized water. Since the MART was located indoors, it was equipped with a VIPARSPECTRA full spectrum aquarium grow light to provide broad spectrum light to the microorganisms inside the tank during experimental days and turned off at night. The grow light was set to a realistic PAR (photosynthetically active radiation) quantity to keep the microorganisms active and not stimulate a bloom. A hollow aluminum coil connected to a water-cooling bath was inserted into the MART to cool the seawater to ~15 ºC to mimic spring ocean temperatures in San Diego. However, during experiments the water warmed (< 5 ºC) due to the heat exhaust from the CFDC chillers located near the MART and cooled again overnight. The centrifugal pump used to recirculate and plunge the water in the MART can damage microorganisms due to strong pump shear (Mayer et al., 2020) and this effect can be highly selective and may change the composition of the biologic community. It is unclear how this affects the microorganisms that are directly emitted as SSA and subsequent ice nucleating ability, but this impact has existed in prior MART studies of freezing by nascent SSA (McCluskey et al., 2018a). MART plunging was turned on shortly after the icing stage of the CFDC (discussed in section 2.3, about 30 minutes before measurement) to ensure aerosol concentrations had equilibrated in all the lines prior to the ice nucleation experiments.

2.2 SSA and SMA generation and characteristics

Aerosol generation from the MART is accomplished by intermittently plunging a sheet of water on top of the water surface, producing a plume of bubbles with a distribution similar to those measured in the ocean. The subsequent polydisperse aerosol size distribution produced from the bursting of bubbles at the water surface closely resembles that which is produced from ocean wave breaking in the ambient environment (Mayer, et al., 2020). The sealed headspace of the MART containing both aerosols and any emitted gases was modestly pressurized by a zero-air generator (ZAG) pumping 7 liters per minute by volume (LPM_v) into the MART and forcing out the sample air.

Upon exiting the MART, the aerosol sample line split in two, with one sample line sent through two silica gel diffusion dryers to the upstream set of sizing instruments to confirm the nascent SSA number size distributions produced by the MART. The other sample line was passed through the OFR, whether powered to produce oxidation or not (see below), for further processing and characterization of ice nucleation behavior, to ensure aerosol losses were consistent during all the experiments. The OFR generates high concentrations of O_3 and OH radicals to oxidize particles using two UV lamps at wavelengths λ = 254 nm and λ =184 nm (Mayer et al., 2020). The two wavelengths were used at a 90:10 ratio, with 90 % intensity from λ = 254 and 10 % from λ =184 nm. An O_3 monitor measured concentrations ~0.7 ppm inside the OFR, a value representative of ~4–6 days of atmospheric aging. In addition, the RH inside the OFR was maintained > 60 % to ensure OH chemistry dominated the oxidation processes and minimize O-singlet reactions. Sample air exiting the OFR first passed through a Nafion dryer, which used ~10 LPM_v of counter flow in its dry air circuit to dehydrate the sample air. After drying, sample air was passed through a diffusion dryer packed with Carulite, an O_3 destroying catalyst, to remove residual O_3 and then passed through a final 4-way split: 1) molecular sieves dryer and CFDC, 2) second set of sizing instruments, 3) ice spectrometer filter (IS), and 4) RH monitor and excess flow vent (Figure 1). The RH monitor confirmed the aerosol stream RH was generally <10 % for all experiments, so aerosol size distribution measurements and IS filter collections were considered to be dry.

Three different aerosol types were generated and investigated for both natural and artificial seawater, depending on whether the MART plunging and OFR were active (see Table 1). The generation, oxidation, sizing and flow configuration was the exact same for both water types. The three aerosol types were 1) primary or freshly emitted SSA (pSSA), 2) “aged” (or oxidized) SSA and SMA (aSSA+SMA, henceforth), and 3) SMA (SMA-only). We hypothesize SMA is formed mostly through the oxidation of DMS, similar to Mayer et al., (2020b), who showed that sulfates contributed to > 50 % of the mass of SMA generated from real seawater in a MART. Two duplicate CFDC experiments were conducted for both pSSA and aSSA+SMA measurements, while only one

https://doi.org/10.5194/egusphere-2023-1016
Preprint. Discussion started: 14 June 2023

experiment was conducted for SMA-only. Between the artificial and natural seawater experiments, the MART was cleaned and filled with DI water and a "blank" experiment was conducted to test background contamination. This experiment was conducted the same as the SMA experiments where the MART plunging was turned off and only the MART headspace was sampled.

Size distributions of the aerosol samples were measured using a combination of a Scanning Mobility Particle Sizer (SMPS, TSI models 3080, 3081, 3010; 12-600 nm) and an Aerodynamic Particle Sizer (APS, TSI model 3321; 0.52 – 20 µm). For this study, two sets of aerosol sizing instruments were used, one located upstream of the OFR, and one located downstream of the OFR, Nafion, and Carulite dryers (see Figure 1). Measurements from the downstream set were used to quantify the sample losses that occurred inside the OFR and dryers. Size distributions comparing both upstream and downstream sets of sizing instruments can be found in the Supplementary Figure S1 and represent an average of the SMPS and APS scans over the course of each ice nucleation experiment, ~4 hours. The APS measurements were converted from aerodynamic to geometric diameter using a dynamic shape factor and particle density of SSA of 1.05 and 1.9 g m^{-3}, respectively, consistent with values from observations and those applied in previous studies (Brock et al., 2019; Patnaude et al., 2021; Zieger et al., 2017).

Data from the SMPS and APS were merged into a complete size distribution, as shown in Figure 2 for all experiments. The solid lines indicate aerosols generated from real seawater and the dashed lines are those generated from artificial seawater. It is clear for sizes < 200 nm that the aSSA+SMA distributions were dominated by secondary particle formation, as indicated by their similarity to the SMA-only experiment. Both aSSA+SMA distributions agree with the pSSA distributions at larger sizes, however this occurs at different aerosol diameters for the ASW and SW, where the distributions begin to converge at ~200 nm and 1 µm for the ASW and SW, respectively. This is consistent with previous work that showed only a small fraction of the submicron aSSA+SMA number distribution generated from a MART originated from the pSSA (Mayer et al., 2020b; Prather et al., 2013). Mayer et al., (2020b) also suggested that new particle nucleation was favored over condensation in the OFR due to the high OH concentrations and fast oxidation rates. However, the higher concentration of aSSA+SMA compared to pSSA from natural SW between 200 nm and 1 µm (Figure 2b) suggests some modification of the pSSA. This could occur through a number of different factors, including gas-phase condensation, changes to the seawater microbial activity altering emissions, or minor changes to particle generation due to surface tension or temperature. The SW size distributions had higher concentrations of aSSA+SMA than the ASW < 100 nm, which may indicate additional gas phase emissions capable of oxidizing to condensable species. Both pSSA size distributions showed peaks around 100 nm, in agreement with other studies that generated SSA in laboratory settings (Collins et al., 2014; Patnaude et al., 2021; Quinn et al., 2015). However, there was a slight secondary mode at ~800 nm that only occurred during the real seawater experiments (Figure 2b). This may represent additional aerosolized biologic material such as bacteria that would not exist in the ASW and may explain lower concentrations in the aSSA+SMA generated from ASW compared to SW between 200 nm and 1 µm. The differences in the ~800 nm mode could also be due to modifications in droplet generation mechanisms, through small differences in temperature, RH, and surfactant content (Stokes et al., 2013). For the blank (background) tests with DI water, with the OFR turned on (black line), it was found that there was also secondary particle formation, likely a result of VOCs emitted from the acrylic material of the MART walls. Hence, the proportion of secondary particles or condensable material formed in the SMA-only and aSSA+SMA cases that was contributed from direct gas-phase emission from the SW and ASW, compared to other organics from the acrylic outgassing, cannot be determined. It is likely that the outgassing of acrylic materials varies with temperature, which could contribute to some of the differences observed in the aSSA+SMA and SMA-only size distributions. Future studies will need to probe SMA ice nucleation by using non-plastic materials. We will nevertheless assume the role of SMA can be interpreted from the ice nucleation experiments, as will be discussed in the subsequent results sections. As a final note, for the blank test the water was not cooled as in the SW and ASW experiments due to time constraints, which likely led to higher VOC emissions and secondary particle concentrations. A similar trend was observed during the pSSA and aSSA+SMA experiments,

https://doi.org/10.5194/egusphere-2023-1016
Preprint. Discussion started: 14 June 2023

where higher particle concentrations were also observed later in the experiments due to the warming of the water with time (Figure S2).

The phase state of the particles before entering the CFDC remains uncertain and could affect the heterogeneous nucleating ability of the aerosol population. Several previous studies have analyzed the temperature- and humidity-dependent phase states of NaCl particles, since they are often used as a proxy for SSA. One study found that the phase state of NaCl after efflorescence depends on the temperature at which efflorescence occurred, with anhydrous NaCl observed for efflorescence temperatures above 273 K (Koop et al., 2000). However, the phase state and morphology are less well understood at low temperatures, and the exact structure was uncertain in this study. This is especially difficult to know for the aSSA+SMA particles, due to the exposure to oxidation in the OFR. On the one hand, aerosols that contain organic material may form a porous glassy state and either enhance heterogeneous nucleation (Adler et al., 2013; Wilson et al., 2012) or have no effect (Kasparoglu et al., 2022). On the other hand, organic coatings on mineral dust particles have been shown to suppress heterogeneous nucleation to higher RH at cirrus temperatures (Möhler et al., 2008), depending also on the coating thickness or the fractional coverage of the particles, while another study found organic coatings on mineral dust had no effect on immersion freezing between 253–233 K regardless of the coating thickness (Kanji et al., 2019). As mentioned previously, the OFR favors new particle formation over condensation on existing SSA particles, however some alterations (addition or functional group alteration) of the SSA organic content cannot be discounted.

2.3 Ice nucleation detection using the CFDC

Detection of low temperature ice nucleation for all experiments was carried out using a CSU CFDC, which had been modified from the design used in previous studies (Archuleta et al., 2005; DeMott et al., 2015; DeMott et al., 2009) to reach temperatures down to 190 K. A full description of the modifications made to the CFDC to reach lower temperatures, and a complete derivation of calculations and measurement uncertainties can be found in Patnaude et al., (2021). The CFDC is made up of two vertically-oriented concentric cylinders consisting of a “cold” inner wall and “warm” outer wall. The chamber temperature and relative humidity (RH) are controlled by holding the inner and outer walls at different temperatures, producing temperature and water partial pressure gradients. This approach can produce a very broad range of RH conditions as low as 0 % with respect to ice and up to double digit supersaturations with respect to water (Rogers, 1988). The walls are covered with a thin layer of ice by chilling the column to 246 K and filling, then draining, the column with deionized water prior to ice nucleation experiments. The flow rates during experiments were 4 LPM_v sheath flow and 1 LPM_v sample flow (calculated in the CFDC interior). The low sample flow translates to a longer residence time inside the CFDC, allowing for more ice crystal growth and thus less ambiguous optical detection of ice crystals versus much smaller unfrozen aerosol particles. An optical particle counter (OPC) is located immediately downstream of the CFDC column at its base and freezing of aerosol particles is distinguished by analyzing the number of particles, presumed to be ice crystals, above a certain size.

Careful attention was given to the challenging identification of slow-growing ice crystals, without incorrectly classifying large aerosols as ice, when using a polydisperse aerosol size distribution and without the presence of an aerosol impactor upstream of the CFDC to remove large particles from the sample stream. In this study, it was not sufficient to only use a single OPC cut size at all temperatures for identifying ice crystals for two reasons: 1) the larger salt particles may undergo significant hygroscopic growth into the size range of ice crystals at RHs above their deliquescence point , and 2) Patnaude et al., (2021) demonstrated the lack of size dependence on the freezing of SSA, meaning the smaller salt particles would likely freeze along with the larger particles and may not be counted if they are below the OPC cut size. Instead, we analyzed the OPC size distributions for increasing RHs, as shown in Figure 3, and identified the background aerosol distributions when the RH is lower, but after deliquescence has likely occurred. Figure 3a shows the OPC size distributions at -45 ºC for pSSA generated from SW and shows

https://doi.org/10.5194/egusphere-2023-1016
Preprint. Discussion started: 14 June 2023

little change in the distribution until the RH reaches 99 % (green line) where a significant number of larger particles emerged, signifying ice nucleation was occurring. At the lower RHs (< 95 %) the salt particles in the seawater would have already deliquesced and taken up water, and therefore these distributions represent the background aerosol population that would need to be removed to count the total number of ice crystals. The lack of change in the size distributions between 80–90 % may be due to smaller SSA growth factors below 95 % (Tang et al., 1997), or kinetic limitations at these temperatures. Figure 3b shows another example of the OPC distributions for measurements at -68 ºC. In this case, there was a much more considerable shift in the distributions with increasing RH, more likely due to ice nucleation and to a lesser extent from hygroscopic growth. When comparing the two temperatures (Figures 3a and b), the distributions in Figure 3b below 75 % (blue and red lines) closely match the lower RH distributions in Figure 3a, indicating they are likely the background aerosols at this temperature and that the additional shift to larger sizes for RHs > 75 % was a result of particles freezing. Based on this analysis we used bin channel 40 on the OPC as the lower (more conservative) threshold for ice, which from previous calibrations represents particles ~2 µm for a flow rate of 5 LPM_v, where roughly 0.1 % of the dry aerosol particles are present (see Figure S1). Therefore, the total number of ice crystals is calculated as the difference between the OPC spectra and background aerosol distributions summed above channel 40 (denoted by the blue shaded region in Figure 3). This method considers both the nucleation of smaller particles and eliminates larger particles that have not nucleated ice.

2.4 Ice Spectrometer measurements of INPs

To sample INPs in the mixed phase regime (-38–0 ºC), an inline Pall IS filter unit was placed downstream of the 4-way split (Figure 1). It was fitted with a 47 mm-diameter 0.05 µm-pore-diameter Nuclepore track-etched polycarbonate membrane (Whatman, Cytiva) overlying a 10 µm-pore-diameter Nuclepore membrane (as a clean support). The flow rate was ~2 standard LPM (21.1 °C, 101.3 kPa), measured with a TSI 5200 flow meter during sampling periods (3–4 hours). Details of the filter unit cleaning procedure is given in McCluskey et al. (2017) and the filter cleaning method in Barry et al., (2021). All steps were carried out in a laminar flow cabinet.

To re-suspend collected aerosol, each filter was placed in a 50 mL Falcon tube (Corning), 7 mL of 0.1 µm-filtered deionized water added, and the tube tumbled on a Roto-Torque (Cole-Palmer) for 20 min. INPs were measured in each aerosol suspension, and in 11- and 121-fold dilutions to estimate concentrations of INPs active at colder temperatures (to -28 °C). To estimate INPs, 32×50 µL aliquots of each serial dilution were dispensed into 96-well PCR trays (Optimum Ultra, Life Science Products) in a laminar flow cabinet, and the trays inserted into blocks of the Colorado State University Ice Spectrometer. Immersion freezing temperature spectra per liter of air were obtained as described in Hiranuma et al., (2015). Ninety-five percent confidence intervals were derived from the frozen fraction of wells at each temperature using equation 2 from Agresti and Coull, (1998). A negative control of 0.1 µm-filtered deionized water was included in each measurement to adjust for background INPs in the water used for re-suspensions and dilutions. To account for background INPs on filters, filter blanks (loaded into inline filter units, attached but without flow) were also processed. The number of INPs versus temperature, processed from the IS filters, are shown in Figure S3, and show agreement between the real SW and ASW but on the low end of previous INP measurements generated from a MART (McCluskey et al., 2017).

3. Results and Discussion

In these experiments, the CFDC was operated to perform RH “scans” wherein the column temperature was held constant and the RH_w and RH_i gradually increased until a specified frozen fraction was achieved, in this case 10 %. During an individual scan the

https://doi.org/10.5194/egusphere-2023-1016
Preprint. Discussion started: 14 June 2023

inner wall temperature (T_{IW}) was held constant while the outer wall temperature (T_{OW}) was gradually raised, increasing the column supersaturation. Once 10 % frozen fraction was reached, the T_{IW} was raised 5 K and the T_{OW} was lowered until the frozen fraction dropped below 0.1 %, and the cycle was repeated. Figure 4a shows a time series of CFDC scans for a pSSA experiment. The first three scans that occurred below 220 K showed a gradual increase in ice particle counts (light blue markers) starting around 30 % SS_i, which was indicative of heterogeneous freezing. The final three scans beginning ~218 K, showed a more modest increase in ice particle counts until the SS_i reached nearly 50 %, resulting in a very sharp increase in ice particle counts; these scans indicated cases of homogeneous freezing of the SSA particles. These results were broadly consistent with previously reported freezing behaviors of NaCl particles at temperatures between 215 K and 235 K (Patnaude et al., 2021; Wagner et al., 2018). Ice nucleation experiments illustrating CFDC scans for SMA-only generated from sampling the headspace over real seawater are shown in Figure 4b. In this case, all the scans showed little ice formation (< 1 L^{-1}) until the SS_i reached > 50 %, where there was a sudden and rapid onset of freezing of nearly all the aerosol particles. These cases illustrate that SMA froze through a homogeneous freezing mechanism, as there was almost no ice formed until the SS_i reached the expected homogeneous freezing threshold (Koop et al., 2000). The CFDC RH scanning procedure was modified for the SMA cases and is the reason for the slower increase in RH after ice is initially formed. Additionally, most of the SMA particles formed are below the minimum size of detection of the OPC (~300 nm), therefore the sharp increase in total particles (black line) is mostly a result of the particles freezing and growing to sizes that can be detected by the OPC.

The ice nucleating ability of pSSA and aged aSSA+SMA generated from the MART is examined in Figure 5. The fractions of frozen particles at 1 % and 5 % are shown in T – RH_w space. The frozen fraction was calculated by dividing the CFDC OPC-measured ice concentrations (discussed previously) by the integrated total particle counts measured in the second set of sizing instruments (post-OFR losses). The sizing instruments provided a total aerosol count, since the OPC may not have detected the smallest particles at its lower size bound (~0.3 microns) even at RH exceeding expected deliquescence RH, particularly for the SMA experiments. For calculations of frozen fraction for the aSSA+SMA experiments, the pSSA size distributions were used with the assumption that pSSA would freeze first. The colored markers denote 1 % (blue) and 5 % (green) frozen fraction, where the filled and open markers denote the SSA generated from natural and artificial seawater, respectively. The reference lines indicate ice saturation (black dashed), homogeneous freezing calculated from Koop et al., (2000) (black solid), and the estimated pore condensation RH for an 11 nm pore size (Marcolli, 2014) (yellow solid), as in Patnaude et al. (2021).

For temperatures > 218 K, the majority of both pSSA and aSSA+SMA particles froze at conditions near the threshold expected for homogeneous freezing (Koop et al., 2000). Interestingly, both 1 % and 5 % frozen fractions of pSSA, and 5 % frozen fraction of aSSA+SMA, closely follow the upper bound of the expected homogeneous freezing parameterizations for aqueous sulfuric acid particles (Schneider et al., 2021b) as temperatures decrease from 230 K to 217K. 1 % frozen fractions of aSSA+SMA particles followed the Koop et al., (2000) average homogeneous freezing conditions more closely, within the range of uncertainties for calculation of RH_w in the CFDC (4 %) (Richardson, 2009). Results for 0.1 % frozen fraction (Figure S4) indicated that a small fraction of the aerosol population still froze via heterogeneous nucleation at temperatures warmer than 218 K, with RH_w ~5-10 % lower than the 1 % observations. However, they still fell within the lower uncertainty bounds suggested by Schneider et al., (2021) for freezing of aqueous sulfuric acid. The 0.1 % frozen fraction for particles generated from natural seawater also occurred at lower RH_w (by up to 5 %) than for those from artificial seawater, perhaps indicating the inclusion of a more active subset of organic INPs in the real seawater. One might expect these more effective immersion freezing INPs to be present in concentrations that could be inferred from higher temperature freezing data, and if contained within the overall SSA population, their freezing conditions should parallel homogeneous freezing conditions but with a water activity offset (Archuleta et al., 2005).

https://doi.org/10.5194/egusphere-2023-1016
Preprint. Discussion started: 14 June 2023

During the pSSA experiments the total aerosol concentrations were ~140 cm^{-3}, therefore 0.1 % of the aerosol population would be 140 L^{-1}. When extending the immersion freezing line to water saturation (water activity = 1), as shown in Figure S5, the number of INPs per liter from the IS spectra at those temperatures, ~0.005 L^{-1} at 251 and ~0.5 L^{-1} at 245 K for SW and ASW, respectively, was much lower than reflected by 0.1 % freezing of all particles at lower temperatures. Therefore, we did not observe the expected number of heterogeneous freezing INPs based on the IS spectra (Figure S3). We do not understand the exact mechanism for the freezing of the lower fractions of particles in the temperature regime where homogeneous freezing dominates. In other words, the 0.1 % frozen fraction is not consistent (higher than) the expected contribution of immersion freezing of the more specialized INPs that are present in SSA for mixed-phase temperatures (when using the water activity freezing concept).

Below 218 K, the onset of freezing for both pSSA and aSSA+SMA occurred at much lower RH_w, ~70 %, for both the artificial and real seawater experiments. This shift from homogeneous freezing to heterogeneous freezing for the major proportion of particles at temperatures below ~220 K was consistent with several previous experiments investigating the freezing of NaCl and SSA particles (Ladino et al., 2016; Patnaude et al., 2021; Schill & Tolbert, 2014; Wagner et al., 2018; Wolf et al., 2019; 2020a). Additionally, for both water types, the onset of heterogeneous freezing occurred near the estimated deliquescence RHs of NaCl and SSA (blue shaded region), similar to the results in previous studies (Patnaude et al., 2021; Wagner et al., 2018, 2021). The deliquescence RH of NaCl was estimated for colder temperatures from Tang & Munkelwitz, (1993), and was lowered ~4 % RH for SSA following Wagner et al., (2018) with the assumption that the additional salts in seawater would deliquesce at a lower RH. The observations in Figure 5 also demonstrated that there was little to no effect on the ice nucleating ability of SSA after undergoing simulated atmospheric aging. Both the pSSA and aSSA+SMA results showed that a transition from primarily homogeneous freezing to heterogeneous nucleation occurred at ~218 K.

In contrast to the ice nucleation results for pSSA and aSSA+SMA, the SMA generated by sampling and oxidizing the gases in the headspace of the MART, over both artificial and natural seawater samples, showed no indication of heterogeneous nucleation at any temperature (Figure 6; 1 % frozen fraction shown). For SMA generated from a combination of emissions and acrylic VOCs from both water types, 1 % frozen fraction did not occur until RH_w had almost reached water saturation, well above the expected freezing threshold for homogeneous nucleation. Due to the rapid onset of ice particle formation as the RH_w was increased beyond the homogeneous freezing threshold, 1 % was the lowest fraction that could be reliably detected by the OPC. These results support the conclusion that pure SMA does not freeze via heterogeneous nucleation at cirrus temperatures, similar to previous studies that analyzed the ice nucleating ability of non-marine SOA in the cirrus regime (Kasparoglu et al., 2022).

4. Conclusions

In this study, a MART provided a representative method for generating polydisperse SSA for comparison to our prior studies of monodisperse NaCl and SSA particle freezing at cirrus temperatures (Patnaude et al., 2021). Despite the added complexity from generating a polydisperse SSA distribution, the impact on heterogeneous ice nucleation behavior was minimal. This was illustrated by the striking similarities in ice nucleation results between the pSSA from this study and the results from Patnaude et al., (2021), which both determined that the onset of heterogeneous nucleation for a 1 % frozen fraction occurred at ~218 K. The results from this current study also corroborate the association of the transition from homogeneous to heterogeneous nucleation at these cirrus temperatures with the presence of crystallized (undissolved) salts in pSSA, and with no demonstrated size dependence.

The results in this study specifically address questions raised by Wagner et al., (2021): will a higher number of ice-active particles be generated from a sea spray chamber where highly organic particles may be formed (Wilson et al., 2015; Wolf et al., 2020); or, if highly organic-rich particles are present, would these particles be aerosolized when generated in a more realistic manner? It is

https://doi.org/10.5194/egusphere-2023-1016
Preprint. Discussion started: 14 June 2023

possible that organic particles in the pSSA from real seawater may contribute a small additional subset of the INP population and freeze more efficiently at warmer temperatures, as shown by the observed 0.1 % frozen fraction at much lower RH_w above 220 K than the 1 % or 5 % frozen fractions (Figure S4). Additionally, the 0.1 % frozen fraction from natural SW has RH_w up to 5 % lower than the 0.1 % results from ASW, which may also be a result of organic enrichment. Organic-rich particles may not deliquesce until higher RHs (>80 %), allowing for heterogeneous nucleation under these conditions, whereas pure salt particles would be fully dissolved and would not freeze until the homogeneous freezing threshold is reached. However, even if these are organic-enriched or internally mixed particles and represent a subset of the INPs in marine aerosols at cirrus levels, they are vastly outnumbered by the inorganic salt particles that appear to dominate heterogeneous ice nucleation at these temperatures.

No prior studies have investigated how atmospheric aging may impact SSA ice nucleation at cirrus temperatures. This study showed that atmospheric aging of pSSA and the formation of an additional SMA population via new particle formation (simulated by use of an OFR) did not affect the ice nucleating behavior of the emitted particles, as demonstrated by the similar results obtained with both pSSA and aSSA+SMA. These results also indicate that secondary particle formation from the gas-phase emissions of natural seawater does not generate effective INPs at cirrus temperatures, as the SMA-only case did not reach 1 % frozen fraction until the RH_w had almost reached water saturation. Thus, SMA may only be considered a relevant source for ice nucleation in cirrus clouds if they are exposed to a pathway that begins via activation as a CCN into cloud droplets at lower altitudes, lofted to cirrus temperatures in deep convection, and then freeze homogeneously (liquid-origin cirrus, see Krämer et al., (2020) and Luebke et al., (2016)).

This study could not distinguish whether the experiments were affected by any of the following: changes to the phase state or morphology of the aSSA+SMA particles; whether fragmentation of aerosol-phase organic compounds occurred; or if glassy states were induced. Exploring these possibilities would require that associated compositional studies be aligned with similar experiments (Mayer et al., 2020b; Prather et al., 2013), but these results suggested that the strongest heterogeneous freezing behaviors noted at temperatures below 218 K were dominated by the salt components even after atmospheric aging. One remaining caveat to this study regarding the SMA and aSSA+SMA results is the uncertainty of the contribution from the seawater versus outgassing from the MART to the mass of secondary material produced, which should be addressed by future studies that might also include compositional and phase state data.

We have shown SSA can nucleate ice via heterogeneous nucleation below 220 K. Airborne observations have found concentrations of sea salt between 10^{-4} – 10^{-1} μg m^{-3} in the upper troposphere (Bian et al., 2019; Murphy et al., 2019), and based on the results shown herein a large proportion of those salt particles should retain their ice nucleating ability even after the atmospheric aging that would occur during their ascent to cirrus levels. Cirrus clouds are ubiquitous in the upper troposphere and represent a large source of uncertainty in determining Earth's radiative budget. In addition, cirrus clouds that form via heterogeneous nucleation have also been shown to represent a net positive radiative forcing (Krämer et al., 2020), thus demonstrating a potential indirect radiative effect of SSA on our climate system.

Author contributions

R. Patnaude, P. DeMott, S. Kreidenweis contributed to the development of the ideas, quality controlled the data, and wrote the majority of the manuscript. R. Patnaude contributed to the analysis of the data. K. Moore and R. Perkins performed the majority of the experimental setup and contributed to the experimental design and execution. T. Hill contributed to the cleaning, preparation, and collection of the IS filters. All coauthors contributing to reviewing and editing of the manuscript.

https://doi.org/10.5194/egusphere-2023-1016
Preprint. Discussion started: 14 June 2023

Competing interests

The authors declare that they have no conflict of interest.

Code and data availability

Data are provided in the manuscript and will be uploaded as supplemental information in the final version.

Acknowledgements

This work was supported by the National Science Foundation (NSF) through the NSF Center for Aerosol Impacts on Chemistry of the Environment (NSF-CAICE), Award CHE-1801971. We would like to acknowledge Matt Pendergraft and Raymond Leibensperger III for their assistance in the seawater collection and shipment to Colorado. K. Moore acknowledges support by an NSF Graduate Research Fellowship under Grant 006784. Any opinions, findings, and conclusions or recommendations expressed in this material are those of the author(s) and do not necessarily reflect the views of the National Science Foundation.

References

Abbatt, J. P. D., Benz, S., Cziczo, D. J., Kanji, Z., Lohmann, U. and Möhler, O.: Solid Ammonium Sulfate Aerosols as Ice Nuclei: A Pathway for Cirrus Cloud Formation, Science (80-.)., 313(5794), 1770–1773, doi:10.1126/science.1129726, 2006.

Adler, G., Koop, T., Haspel, C., Taraniuk, I., Moise, T., Koren, I., Heiblum, R. H. and Rudich, Y.: Formation of highly porous aerosol particles by atmospheric freeze-drying in ice clouds, Proc. Natl. Acad. Sci., 110(51), 20414–20419, doi:10.1073/pnas.1317209110, 2013.

Agresti, A. and Coull, B. A.: Approximate is Better than "Exact" for Interval Estimation of Binomial Proportions, Am. Stat., 52(2), 119–126, doi:10.1080/00031305.1998.10480550, 1998.

Archuleta, C. M., DeMott, P. J. and Kreidenweis, S. M.: Ice nucleation by surrogates for atmospheric mineral dust and mineral dust/sulfate particles at cirrus temperatures, Atmos. Chem. Phys., 5(10), 2617–2634, doi:10.5194/acp-5-2617-2005, 2005.

Baker, M. B.: Cloud microphysics and climate, Science (80-.)., 276(5315), 1072–1078, doi:10.1126/science.276.5315.1072, 1997.

Barry, K. R., Hill, T. C. J., Jentzsch, C., Moffett, B. F., Stratmann, F. and DeMott, P. J.: Pragmatic protocols for working cleanly when measuring ice nucleating particles, Atmos. Res., 250(September 2020), 105419, doi:10.1016/j.atmosres.2020.105419, 2021.

Baustian, K. J., Wise, M. E. and Tolbert, M. A.: Depositional ice nucleation on solid ammonium sulfate and glutaric acid particles, Atmos. Chem. Phys., 10(5), 2307–2317, doi:10.5194/acp-10-2307-2010, 2010.

Berresheim, H., Eisele, F. L., Tanner, D. J., McInnes, L. M., Ramsey-Bell, D. C. and Covert, D. S.: Atmospheric sulfur chemistry and cloud condensation nuclei (CCN) concentrations over the northeastern Pacific Coast, J. Geophys. Res., 98(D7), 12701, doi:10.1029/93JD00815, 1993.

Bian, H., Froyd, K., Murphy, D. M., Dibb, J., Darmenov, A., Chin, M., Colarco, P. R., Da Silva, A., Kucsera, T. L., Schill, G., Yu, H., Bui, P., Dollner, M., Weinzierl, B. and Smirnov, A.: Observationally constrained analysis of sea salt aerosol in the marine atmosphere, Atmos. Chem. Phys., 19(16), 10773–10785, doi:10.5194/acp-19-10773-2019, 2019.

Brock, C. A., Williamson, C., Kupc, A., Froyd, K. D., Erdesz, F., Wagner, N., Richardson, M., Schwarz, J. P., Gao, R. S., Katich, J. M., Campuzano-Jost, P., Nault, B. A., Schroder, J. C., Jimenez, J. L., Weinzierl, B., Dollner, M., Bui, T. and Murphy, D. M.: Aerosol size distributions during the Atmospheric Tomography Mission (ATom): Methods, uncertainties, and data products, Atmos. Meas. Tech., 12(6), 3081–3099, doi:10.5194/amt-12-3081-2019, 2019.

Chen, T., Rossow, W. B. and Zhang, Y.: Radiative effects of cloud-type variations, J. Clim., 13(1), 264–286, doi:10.1175/1520-0442(2000)013<0264:REOCTV>2.0.CO;2, 2000.

https://doi.org/10.5194/egusphere-2023-1016
Preprint. Discussion started: 14 June 2023

Collins, D. B., Zhao, D. F., Ruppel, M. J., Laskina, O., Grandquist, J. R., Modini, R. L., Stokes, M. D., Russell, L. M., Bertram, T. H., Grassian, V. H., Deane, G. B. and Prather, K. A.: Direct aerosol chemical composition measurements to evaluate the physicochemical differences between controlled sea spray aerosol generation schemes, Atmos. Meas. Tech., 7(11), 3667–3683, doi:10.5194/amt-7-3667-2014, 2014.

Cziczo, D. J. and Froyd, K. D.: Sampling the composition of cirrus ice residuals, Atmos. Res., 142, 15–31, doi:10.1016/j.atmosres.2013.06.012, 2014.

Cziczo, D. J., Murphy, D. M., Hudson, P. K. and Thomson, D. S.: Single particle measurements of the chemical composition of cirrus ice residue during CRYSTAL-FACE, J. Geophys. Res. Atmos., 109, D04201, doi:10.1029/2003jd004032, 2004.

Cziczo, D. J., Froyd, K. D., Hoose, C., Jensen, E. J., Diao, M., Zondlo, M. A., Smith, J. B., Twohy, C. H. and Murphy, D. M.: Clarifying the dominant sources and mechanisms of cirrus cloud formation, Science (80-.)., 340(6138), 1320–1324, doi:10.1126/science.1234145, 2013.

David, R. O., Marcolli, C., Fahrni, J., Qiu, Y., Perez Sirkin, Y. A., Molinero, V., Mahrt, F., Brühwiler, D., Lohmann, U. and Kanji, Z. A.: Pore condensation and freezing is responsible for ice formation below water saturation for porous particles, Proc. Natl. Acad. Sci. U. S. A., 116(17), 8184–8189, doi:10.1073/pnas.1813647116, 2019.

DeMott, P. J., Cziczo, D. J., Prenni, A. J., Murphy, D. M., Kreidenweis, S. M., Thomson, D. S., Borys, R. and Rogers, D. C.: Measurements of the concentration and composition of nuclei for cirrus formation, Proc. Natl. Acad. Sci., 100(25), 14655–14660, doi:10.1073/pnas.2532677100, 2003.

DeMott, P. J., Petters, M. D., Prenni, A. J., Carrico, C. M., Kreidenweis, S. M., Collett, J. L. and Moosmüller, H.: Ice nucleation behavior of biomass combustion particles at cirrus temperatures, J. Geophys. Res. Atmos., 114(D16), D16205, doi:10.1029/2009JD012036, 2009.

DeMott, P. J., Prenni, A. J., McMeeking, G. R., Sullivan, R. C., Petters, M. D., Tobo, Y., Niemand, M., Möhler, O., Snider, J. R., Wang, Z. and Kreidenweis, S. M.: Integrating laboratory and field data to quantify the immersion freezing ice nucleation activity of mineral dust particles, Atmos. Chem. Phys., 15(1), 393–409, doi:10.5194/acp-15-393-2015, 2015.

Fitzgerald, J. W.: Marine aerosols: A review, Atmos. Environ. Part A, Gen. Top., 25(3–4), 533–545, doi:10.1016/0960-1686(91)90050-H, 1991.

Froyd, K. D., Murphy, S. M., Murphy, D. M., De Gouw, J. A., Eddingsaas, N. C. and Wennberg, P. O.: Contribution of isoprene-derived organosulfates to free tropospheric aerosol mass, Proc. Natl. Acad. Sci. U. S. A., 107(50), 21360–21365, doi:10.1073/pnas.1012561107, 2010.

Hiranuma, N., Augustin-Bauditz, S., Bingemer, H., Budke, C., Curtius, J., Danielczok, A., Diehl, K., Dreischmeier, K., Ebert, M., Frank, F., Hoffmann, N., Kandler, K., Kiselev, A., Koop, T., Leisner, T., Möhler, O., Nillius, B., Peckhaus, A., Rose, D., Weinbruch, S., Wex, H., Boose, Y., Demott, P. J., Hader, J. D., Hill, T. C. J., Kanji, Z. A., Kulkarni, G., Levin, E. J. T., McCluskey, C. S., Murakami, M., Murray, B. J., Niedermeier, D., Petters, M. D., O'Sullivan, D., Saito, A., Schill, G. P., Tajiri, T., Tolbert, M. A., Welti, A., Whale, T. F., Wright, T. P. and Yamashita, K.: A comprehensive laboratory study on the immersion freezing behavior of illite NX particles: A comparison of 17 ice nucleation measurement techniques, Atmos. Chem. Phys., 15(5), 2489–2518, doi:10.5194/acp-15-2489-2015, 2015.

Hoose, C. and Möhler, O.: Heterogeneous ice nucleation on atmospheric aerosols: A review of results from laboratory experiments., 2012.

Ickes, L., Porter, G. C. E., Wagner, R., Adams, M. P., Bierbauer, S., Bertram, A. K., Bilde, M., Christiansen, S., Ekman, A. M. L., Gorokhova, E., Höhler, K., Kiselev, A. A., Leck, C., Möhler, O., Murray, B. J., Schiebel, T., Ullrich, R. and Salter, M. E.: The ice-nucleating activity of Arctic sea surface microlayer samples and marine algal cultures, Atmos. Chem. Phys., 20(18), 11089–11117, doi:10.5194/acp-20-11089-2020, 2020.

Jensen, E. J., Kinne, S. and Toon, O. B.: Tropical cirrus cloud radiative forcing: Sensitivity studies, Geophys. Res. Lett., 21(18), 2023–2026, doi:10.1029/94GL01358, 1994.

Kanji, Z. A. and Abbatt, J. P. D.: Ice Nucleation onto Arizona Test Dust at Cirrus Temperatures: Effect of Temperature and Aerosol Size on Onset Relative Humidity, J. Phys. Chem. A, 114(2), 935–941, doi:10.1021/jp908661m, 2010.

Kanji, Z. A., Sullivan, R. C., Niemand, M., DeMott, P. J., Prenni, A. J., Chou, C., Saathoff, H. and Möhler, O.: Heterogeneous ice nucleation properties of natural desert dust particles coated with a surrogate of secondary organic aerosol, Atmos. Chem. Phys., 19(7), 5091–5110, doi:10.5194/acp-19-5091-2019, 2019.

Kärcher, B., DeMott, P. J., Jensen, E. J. and Harrington, J. Y.: Studies on the Competition Between Homogeneous and Heterogeneous Ice Nucleation in Cirrus Formation, J. Geophys. Res. Atmos., 127(3), 1–21, doi:10.1029/2021JD035805, 2022.

Kasparoglu, S., Perkins, R., Ziemann, P. J., DeMott, P. J., Kreidenweis, S. M., Finewax, Z., Deming, B. L., DeVault, M. P. and

https://doi.org/10.5194/egusphere-2023-1016
Preprint. Discussion started: 14 June 2023

Petters, M. D.: Experimental Determination of the Relationship Between Organic Aerosol Viscosity and Ice Nucleation at Upper Free Tropospheric Conditions, J. Geophys. Res. Atmos., 127(16), 1–20, doi:10.1029/2021JD036296, 2022.

Koop, T., Kapilashrami, A., Molina, L. T. and Molina, M. J.: Phase transitions of sea-salt/water mixtures at low temperatures: Implications for ozone chemistry in the polar marine boundary layer, J. Geophys. Res. Atmos., 105(D21), 26393–26402, doi:10.1029/2000JD900413, 2000a.

Koop, T., Luo, B., Tsias, A. and Peter, T.: Water activity as the determinant for homogeneous ice nucleation in aqueous solutions, Nature, 406(6796), 611–614, doi:10.1038/35020537, 2000b.

Krämer, M., Rolf, C., Spelten, N., Afchine, A., Fahey, D., Jensen, E., Khaykin, S., Kuhn, T., Lawson, P., Lykov, A., L. Pan, L., Riese, M., Rollins, A., Stroh, F., Thornberry, T., Wolf, V., Woods, S., Spichtinger, P., Quaas, J. and Sourdeval, O.: A microphysics guide to cirrus - Part 2: Climatologies of clouds and humidity from observations, Atmos. Chem. Phys., 20(21), 12569–12608, doi:10.5194/acp-20-12569-2020, 2020.

Ladino, L. A., Yakobi-Hancock, J. D., Kilthau, W. P., Mason, R. H., Si, M., Li, J., Miller, L. A., Schiller, C. L., Huffman, J. A., Aller, J. Y., Knopf, D. A., Bertram, A. K. and Abbatt, J. P. D.: Addressing the ice nucleating abilities of marine aerosol: A combination of deposition mode laboratory and field measurements, Atmos. Environ., 132, 1–10, doi:10.1016/j.atmosenv.2016.02.028, 2016.

Liou, K.-N.: Influence of Cirrus Clouds on Weather and Climate Processes: A Global Perspective, Mon. Weather Rev., 114(6), 1167–1199 [online] Available from: 10.1175/1520-0493(1986)114%3C1167:IOCCOW%3E2.0.CO;2, 1986.

Luebke, A. E., Afchine, A., Costa, A., Grooß, J. U., Meyer, J., Rolf, C., Spelten, N., M Avallone, L., Baumgardner, D. and Krämer, M.: The origin of midlatitude ice clouds and the resulting influence on their microphysical properties, Atmos. Chem. Phys., 16(9), 5793–5809, doi:10.5194/acp-16-5793-2016, 2016.

Marcolli, C.: Deposition nucleation viewed as homogeneous or immersion freezing in pores and cavities, Atmos. Chem. Phys., 14(4), 2071–2104, doi:10.5194/acp-14-2071-2014, 2014.

Mayer, K. J., Sauer, J. S., Dinasquet, J. and Prather, K. A.: CAICE Studies: Insights from a Decade of Ocean-Atmosphere Experiments in the Laboratory, Acc. Chem. Res., 53(11), 2510–2520, doi:10.1021/acs.accounts.0c00504, 2020a.

Mayer, K. J., Wang, X., Santander, M. V., Mitts, B. A., Sauer, J. S., Sultana, C. M., Cappa, C. D. and Prather, K. A.: Secondary Marine Aerosol Plays a Dominant Role over Primary Sea Spray Aerosol in Cloud Formation, ACS Cent. Sci., 6(12), 2259–2266, doi:10.1021/acscentsci.0c00793, 2020b.

McCluskey, C. S., Hill, T. C. J., Malfatti, F., Sultana, C. M., Lee, C., Santander, M. V., Beall, C. M., Moore, K. A., Cornwell, G. C., Collins, D. B., Prather, K. A., Jayarathne, T., Stone, E. A., Azam, F., Kreidenweis, S. M. and DeMott, P. J.: A Dynamic Link between Ice Nucleating Particles Released in Nascent Sea Spray Aerosol and Oceanic Biological Activity during Two Mesocosm Experiments, J. Atmos. Sci., 74(1), 151–166, doi:10.1175/JAS-D-16-0087.1, 2017.

McCluskey, C. S., Hill, T. C. J., Sultana, C. M., Laskina, O., Trueblood, J., Santander, M. V., Beall, C. M., Michaud, J. M., Kreidenweis, S. M., Prather, K. A., Grassian, V. and DeMott, P. J.: A Mesocosm Double Feature: Insights into the Chemical Makeup of Marine Ice Nucleating Particles, J. Atmos. Sci., 75(7), 2405–2423, doi:10.1175/JAS-D-17-0155.1, 2018a.

McCluskey, C. S., Hill, T. C. J., Humphries, R. S., Rauker, A. M., Moreau, S., Strutton, P. G., Chambers, S. D., Williams, A. G., McRobert, I., Ward, J., Keywood, M. D., Harnwell, J., Ponsonby, W., Loh, Z. M., Krummel, P. B., Protat, A., Kreidenweis, S. M. and DeMott, P. J.: Observations of Ice Nucleating Particles Over Southern Ocean Waters, Geophys. Res. Lett., 45(21), 11,989-11,997, doi:10.1029/2018GL079981, 2018b.

Möhler, O., Benz, S., Saathoff, H., Schnaiter, M., Wagner, R., Schneider, J., Walter, S., Ebert, V. and Wagner, S.: The effect of organic coating on the heterogeneous ice nucleation efficiency of mineral dust aerosols, Environ. Res. Lett., 3(2), doi:10.1088/1748-9326/3/2/025007, 2008.

Murphy, D. M., Froyd, K. D., Bian, H., Brock, C. A., Dibb, J. E., Digangi, J. P., Diskin, G., Dollner, M., Kupc, A., Scheuer, E. M., Schill, G. P., Weinzierl, B., Williamson, C. J. and Yu, P.: The distribution of sea-salt aerosol in the global troposphere, Atmos. Chem. Phys., 19(6), 4093–4104, doi:10.5194/acp-19-4093-2019, 2019.

O'Dowd, C. D. and De Leeuw, G.: Marine aerosol production: A review of the current knowledge, Philos. Trans. R. Soc. A Math. Phys. Eng. Sci., 365(1856), 1753–1774, doi:10.1098/rsta.2007.2043, 2007.

O'Dowd, C. D., Facchini, M. C., Cavalli, F., Ceburnis, D., Mircea, M., Decesari, S., Fuzzi, S., Young, J. Y. and Putaud, J. P.: Biogenically driven organic contribution to marine aerosol, Nature, 431(7009), 676–680, doi:10.1038/nature02959, 2004.

Pandis, S. N., Russell, L. M. and Seinfeld, J. H.: The relationship between DMS flux and CCN concentration in remote marine regions, J. Geophys. Res., 99(D8), 16945, doi:10.1029/94JD01119, 1994.

Patnaude, R. J., Perkins, R. J., Kreidenweis, S. M. and DeMott, P. J.: Is Ice Formation by Sea Spray Particles at Cirrus

https://doi.org/10.5194/egusphere-2023-1016
Preprint. Discussion started: 14 June 2023

Temperatures Controlled by Crystalline Salts?, ACS Earth Sp. Chem., 5(9), 2196–2211, doi:10.1021/acsearthspacechem.1c00228, 2021.

Peng, Z. and Jimenez, J. L.: Radical chemistry in oxidation flow reactors for atmospheric chemistry research, Chem. Soc. Rev., 49(9), 2570–2616, doi:10.1039/C9CS00766K, 2020.

Petzold, A., Ström, J., Ohlsson, S. and Schröder, F. P.: Elemental composition and morphology of ice-crystal residual particles in cirrus clouds and contrails, Atmos. Res., 49(1), 21–34, doi:10.1016/S0169-8095(97)00083-5, 1998.

Prather, K. A., Bertram, T. H., Grassian, V. H., Deane, G. B., Stokes, M. D., DeMott, P. J., Aluwihare, L. I., Palenik, B. P., Azam, F., Seinfeld, J. H., Moffet, R. C., Molina, M. J., Cappa, C. D., Geiger, F. M., Roberts, G. C., Russell, L. M., Ault, A. P., Baltrusaitis, J., Collins, D. B., Corrigan, C. E., Cuadra-Rodriguez, L. A., Ebben, C. J., Forestieri, S. D., Guasco, T. L., Hersey, S. P., Kim, M. J., Lambert, W. F., Modini, R. L., Mui, W., Pedler, B. E., Ruppel, M. J., Ryder, O. S., Schoepp, N. G., Sullivan, R. C. and Zhao, D.: Bringing the ocean into the laboratory to probe the chemical complexity of sea spray aerosol, Proc. Natl. Acad. Sci. U. S. A., 110(19), 7550–7555, doi:10.1073/pnas.1300262110, 2013.

Quinn, P. K., Collins, D. B., Grassian, V. H., Prather, K. A. and Bates, T. S.: Chemistry and Related Properties of Freshly Emitted Sea Spray Aerosol, Chem. Rev., 115(10), 4383–4399, doi:10.1021/cr500713g, 2015.

Richardson, M.: Making Real Time Measurements of Ice Nuclei Concentrations at Upper Tropospheric Temperatures : Extending the Capabilities of the Continuous Flow Diffusion, Colorado State University., 2009.

Rogers, D. C.: Development of a continuous flow thermal gradient diffusion chamber for ice nucleation studies, Atmos. Res., 22(2), 149–181, doi:10.1016/0169-8095(88)90005-1, 1988.

Saliba, G., Chen, C. L., Lewis, S., Russell, L. M., Quinn, P. K., Bates, T. S., Bell, T. G., Lawler, M. J., Saltzman, E. S., Sanchez, K. J., Moore, R., Shook, M., Rivellini, L. H., Lee, A., Baetge, N., Carlson, C. A. and Behrenfeld, M. J.: Seasonal Differences and Variability of Concentrations, Chemical Composition, and Cloud Condensation Nuclei of Marine Aerosol Over the North Atlantic, J. Geophys. Res. Atmos., 125(19), 1–24, doi:10.1029/2020JD033145, 2020.

Sanchez, K. J., Roberts, G. C., Saliba, G., Russell, L. M., Twohy, C., Reeves, M. J., Humphries, R. S., Keywood, M. D., Ward, J. P. and McRobert, I. M.: Measurement report: Cloud processes and the transport of biological emissions affect southern ocean particle and cloud condensation nuclei concentrations, Atmos. Chem. Phys., 21(5), 3427–3446, doi:10.5194/acp-21-3427-2021, 2021.

Sassen, K., Wang, Z. and Liu, D.: Global distribution of cirrus clouds from CloudSat/cloud-aerosol lidar and infrared pathfinder satellite observations (CALIPSO) measurements, J. Geophys. Res. Atmos., 113(D8), D00A12, doi:10.1029/2008JD009972, 2008.

Schill, G. P. and Tolbert, M. A.: Heterogeneous ice nucleation on simulated sea-spray aerosol using Raman microscopy, J. Phys. Chem. C, 118(50), 29234–29241, doi:10.1021/jp505379j, 2014.

Schill, G. P., Froyd, K. D., Bian, H., Kupc, A., Williamson, C., Brock, C. A., Ray, E., Hornbrook, R. S., Hills, A. J., Apel, E. C., Chin, M., Colarco, P. R. and Murphy, D. M.: Widespread biomass burning smoke throughout the remote troposphere, Nat. Geosci., 13(6), 422–427, doi:10.1038/s41561-020-0586-1, 2020.

Schneider, J., Höhler, K., Wagner, R., Saathoff, H., Schnaiter, M., Schorr, T., Steinke, I., Benz, S., Baumgartner, M., Rolf, C., Krämer, M., Leisner, T. and Möhler, O.: High homogeneous freezing onsets of sulfuric acid aerosol at cirrus temperatures, Atmos. Chem. Phys., 21(18), 14403–14425, doi:10.5194/acp-21-14403-2021, 2021a.

Schneider, J., Höhler, K., Wagner, R., Saathoff, H., Schnaiter, M., Schorr, T., Steinke, I., Benz, S., Baumgartner, M., Rolf, C., Krämer, M., Leisner, T. and Möhler, O.: High Homogeneous Freezing Onsets of Sulfuric Acid Aerosol at Cirrus Temperatures, Atmos. Chem. Phys. Discuss., doi:10.5194/acp-2021-319, 2021b.

Schumann, U., Mayer, B., Graf, K. and Mannstein, H.: A Parametric Radiative Forcing Model for Contrail Cirrus, J. Appl. Meteorol. Climatol., 51(7), 1391–1406, doi:10.1175/JAMC-D-11-0242.1, 2012.

Schwarz, J. P., Weinzierl, B., Samset, B. H., Dollner, M., Heimerl, K., Markovic, M. Z., Perring, A. E. and Ziemba, L.: Aircraft measurements of black carbon vertical profiles show upper tropospheric variability and stability, Geophys. Res. Lett., 44(2), 1132–1140, doi:10.1002/2016GL071241, 2017.

Stith, J. L., Twohy, C. H., Demott, P. J., Baumgardner, D., Campos, T., Gao, R. and Anderson, J.: Observations of ice nuclei and heterogeneous freezing in a Western Pacific extratropical storm, Atmos. Chem. Phys., 11(13), 6229–6243, doi:10.5194/acp-11-6229-2011, 2011.

Stokes, M. D., Deane, G. B., Prather, K., Bertram, T. H., Ruppel, M. J., Ryder, O. S., Brady, J. M. and Zhao, D.: A Marine Aerosol Reference Tank system as a breaking wave analogue for the production of foam and sea-spray aerosols, Atmos. Meas. Tech., 6(4), 1085–1094, doi:10.5194/amt-6-1085-2013, 2013.

https://doi.org/10.5194/egusphere-2023-1016
Preprint. Discussion started: 14 June 2023

Tang, I. N. and Munkelwitz, H. R.: Composition and temperature dependence of the deliquescence properties of hygroscopic aerosols, Atmos. Environ. Part A, Gen. Top., 27(4), 467–473, doi:10.1016/0960-1686(93)90204-C, 1993.

Tang, I. N., Tridico, A. C. and Fung, K. H.: Thermodynamic and optical properties of sea salt aerosols, J. Geophys. Res. Atmos., 102(D19), 23269–23275, doi:10.1029/97jd01806, 1997.

Vali, G., DeMott, P. J., Möhler, O. and Whale, T. F.: Technical Note: A proposal for ice nucleation terminology, Atmos. Chem. Phys., 15(18), 10263–10270, doi:10.5194/acp-15-10263-2015, 2015.

Vignati, E., Facchini, M. C., Rinaldi, M., Scannell, C., Ceburnis, D., Sciare, J., Kanakidou, M., Myriokefalitakis, S., Dentener, F. and O'Dowd, C. D.: Global scale emission and distribution of sea-spray aerosol: Sea-salt and organic enrichment, Atmos. Environ., 44(5), 670–677, doi:10.1016/j.atmosenv.2009.11.013, 2010.

Wagner, R. and Möhler, O.: Heterogeneous ice nucleation ability of crystalline sodium chloride dihydrate particles, J. Geophys. Res. Atmos., 118(10), 4610–4622, doi:10.1002/jgrd.50325, 2013.

Wagner, R., Kaufmann, J., Möhler, O., Saathoff, H., Schnaiter, M., Ullrich, R. and Leisner, T.: Heterogeneous Ice Nucleation Ability of NaCl and Sea Salt Aerosol Particles at Cirrus Temperatures, J. Geophys. Res. Atmos., 123(5), 2841–2860, doi:10.1002/2017JD027864, 2018.

Wagner, R., Ickes, L., Bertram, A. K., Els, N., Gorokhova, E., Möhler, O., Murray, B. J., Umo, N. S. and Salter, M. E.: Heterogeneous ice nucleation ability of aerosol particles generated from Arctic sea surface microlayer and surface seawater samples at cirrus temperatures, Atmos. Chem. Phys., 21(18), 13903–13930, doi:10.5194/acp-21-13903-2021, 2021.

Wilson, T. W., Murray, B. J., Wagner, R., Möhler, O., Saathoff, H., Schnaiter, M., Skrotzki, J., Price, H. C., Malkin, T. L., Dobbie, S. and Al-Jumur, S. M. R. K.: Glassy aerosols with a range of compositions nucleate ice heterogeneously at cirrus temperatures, Atmos. Chem. Phys., 12(18), 8611–8632, doi:10.5194/acp-12-8611-2012, 2012.

Wilson, T. W., Ladino, L. A., Alpert, P. A., Breckels, M. N., Brooks, I. M., Browse, J., Burrows, S. M., Carslaw, K. S., Huffman, J. A., Judd, C., Kilthau, W. P., Mason, R. H., McFiggans, G., Miller, L. A., Najera, J. J., Polishchuk, E., Rae, S., Schiller, C. L., Si, M., Temprado, J. V., Whale, T. F., Wong, J. P. S., Wurl, O., Yakobi-Hancock, J. D., Abbatt, J. P. D., Aller, J. Y., Bertram, A. K., Knopf, D. A. and Murray, B. J.: A marine biogenic source of atmospheric ice-nucleating particles, Nature, 525, 234–238, doi:10.1038/nature14986, 2015.

Wise, M. E., Baustian, K. J. and Tolbert, M. A.: Internally mixed sulfate and organic particles as potential ice nuclei in the tropical tropopause region, Proc. Natl. Acad. Sci. U. S. A., 107(15), 6693–6698, doi:10.1073/pnas.0913018107, 2010.

Wise, M. E., Baustian, K. J., Koop, T., Freedman, M. A., Jensen, E. J. and Tolbert, M. A.: Depositional ice nucleation onto crystalline hydrated NaCl particles: A new mechanism for ice formation in the troposphere, Atmos. Chem. Phys., 12(2), 1121–1134, doi:10.5194/acp-12-1121-2012, 2012.

Wolf, M. J., Coe, A., Dove, L. A., Zawadowicz, M. A., Dooley, K., Biller, S. J., Zhang, Y., Chisholm, S. W. and Cziczo, D. J.: Investigating the Heterogeneous Ice Nucleation of Sea Spray Aerosols Using Prochlorococcus as a Model Source of Marine Organic Matter, Environ. Sci. Technol., 53(3), 1139–1149, doi:10.1021/acs.est.8b05150, 2019.

Wolf, M. J., Zhang, Y., Zawadowicz, M. A., Goodell, M., Froyd, K., Freney, E., Sellegri, K., Rösch, M., Cui, T., Winter, M., Lacher, L., Axisa, D., DeMott, P. J., Levin, E. J. T., Gute, E., Abbatt, J., Koss, A., Kroll, J. H., Surratt, J. D. and Cziczo, D. J.: A biogenic secondary organic aerosol source of cirrus ice nucleating particles, Nat. Commun., 11(4834), doi:10.1038/s41467-020-18424-6, 2020a.

Wolf, M. J., Goodell, M., Dong, E., Dove, L. A., Zhang, C., Franco, L. J., Shen, C., Rutkowski, E. G., Narducci, D. N., Mullen, S., Babbin, A. R. and Cziczo, D. J.: A link between the ice nucleation activity and the biogeochemistry of seawater, Atmos. Chem. Phys., 20(23), 15341–15356, doi:10.5194/acp-20-15341-2020, 2020b.

Wylie, D. P., Menzel, W. P., Woolf, H. M. and Strabala, K. I.: Four years of global cirrus cloud statistics using HIRS, J. Clim., 7(12), 1972–1986, doi:10.1175/1520-0442(1994)007<1972:FYOGCC>2.0.CO;2, 1994.

Zhang, Y., MacKe, A. and Albers, F.: Effect of crystal size spectrum and crystal shape on stratiform cirrus radiative forcing, Atmos. Res., 52(1), 59–75, doi:10.1016/S0169-8095(99)00026-5, 1999.

Zieger, P., Väisänen, O., Corbin, J. C., Partridge, D. G., Bastelberger, S., Mousavi-Fard, M., Rosati, B., Gysel, M., Krieger, U. K., Leck, C., Nenes, A., Riipinen, I., Virtanen, A. and Salter, M. E.: Revising the hygroscopicity of inorganic sea salt particles, Nat. Commun., 8, doi:10.1038/ncomms15883, 2017.

https://doi.org/10.5194/egusphere-2023-1016
Preprint. Discussion started: 14 June 2023

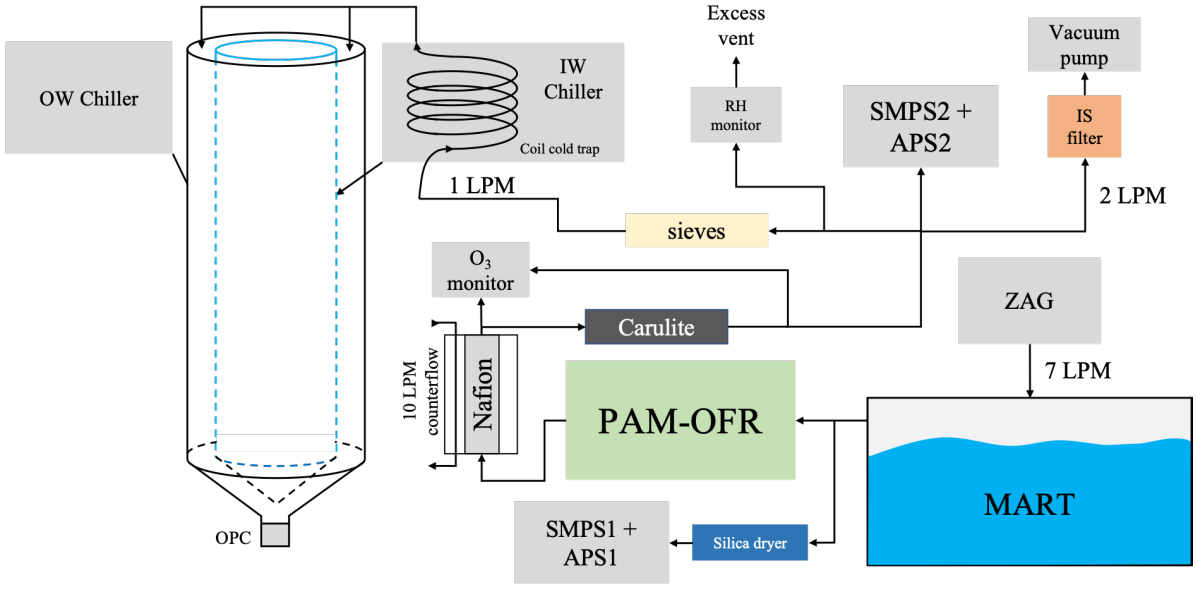

Figure 1. Schematic of the experimental setup for the MART studies. Flow configuration remained the same for all aerosol generation methods and water types.

https://doi.org/10.5194/egusphere-2023-1016
Preprint. Discussion started: 14 June 2023

Table 1. Descriptions of experimental aerosol generated from the MART for each water type.

Generated aerosol types (Water type)	OFR lamp operation	MART plunging
pSSA (ASW, SW)	OFF	ON
aSSA+SMA (ASW, SW)	ON	ON
SMA only (ASW, SW, DI)	ON	OFF

https://doi.org/10.5194/egusphere-2023-1016
Preprint. Discussion started: 14 June 2023

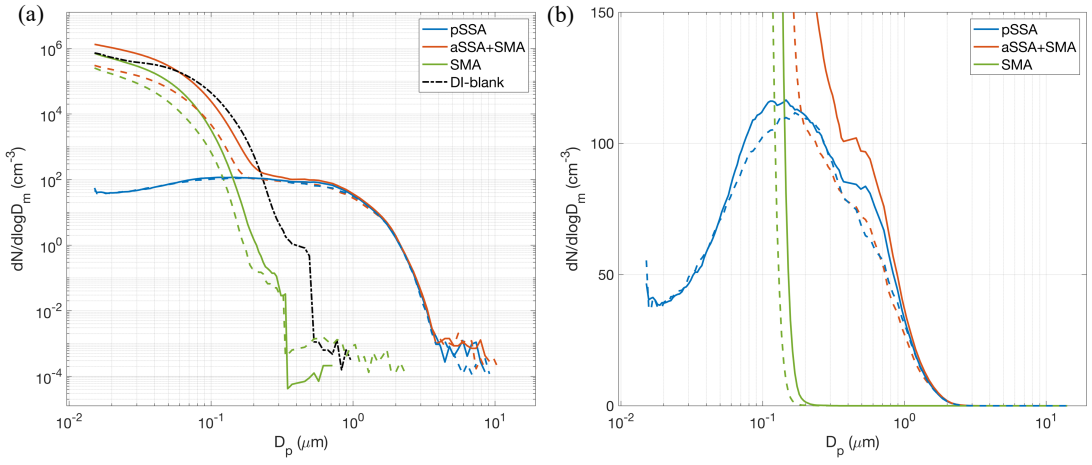

Figure 2. (a) Particle size distributions combined from the SMPS and APS measured downstream of the OFR and (b) the same as (a) but zoomed in a linear axis. The solid lines denote aerosols generated from SW and the dashed lines from ASW. The DI-blank experiment is denoted by the black dashed-dotted line. Size distributions represent a time-average of the SMPS and APS scans measured throughout the entire ice nucleation experiment.

https://doi.org/10.5194/egusphere-2023-1016
Preprint. Discussion started: 14 June 2023

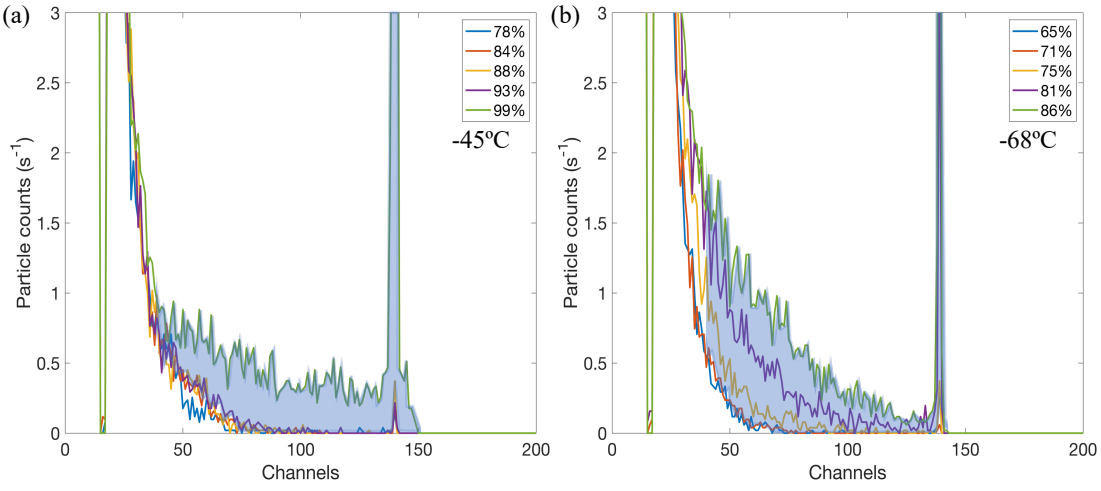

Figure 3. CFDC OPC size distributions of pSSA for increasing RH at (a) -45 ºC and (b) -68 ºC during the first of two real seawater experiments. The blue shaded region represents the difference between OPC counts at higher RHs and counts of background aerosol distributions at lower RHs above channel 40, denoting what would be distinguished as ice particles.

https://doi.org/10.5194/egusphere-2023-1016
Preprint. Discussion started: 14 June 2023

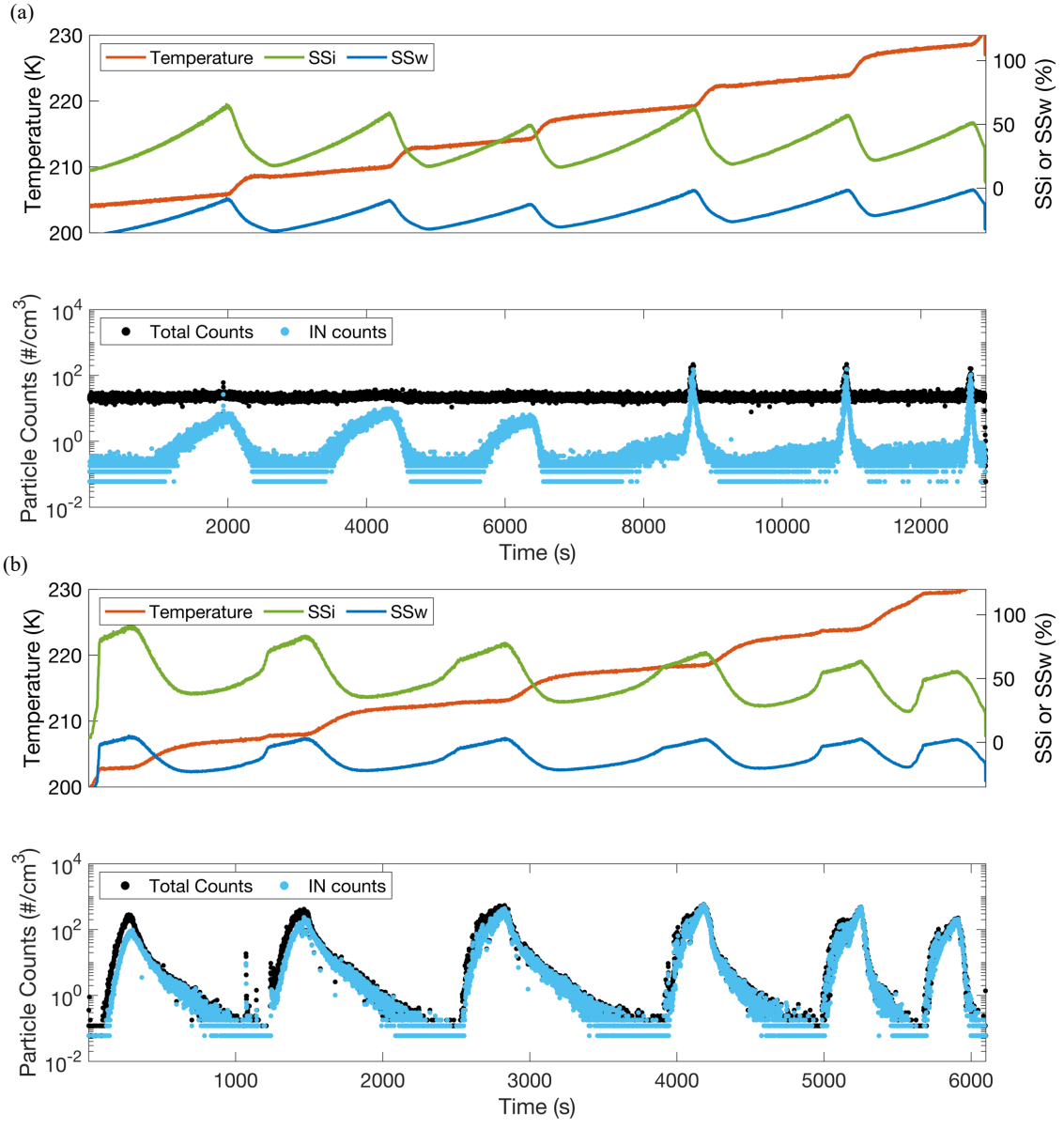

Figure 4. Time series of CFDC scans for (a) pSSA and (b) SMA experiments generated from real seawater beginning at 204 K. Temperature is represented by the red lines, and water and ice supersaturations are represented by the blue and green lines, respectively. The black and light blue markers indicate the numbers of total particles counted in the OPC and those that are considered ice crystals, respectively.

https://doi.org/10.5194/egusphere-2023-1016
Preprint. Discussion started: 14 June 2023

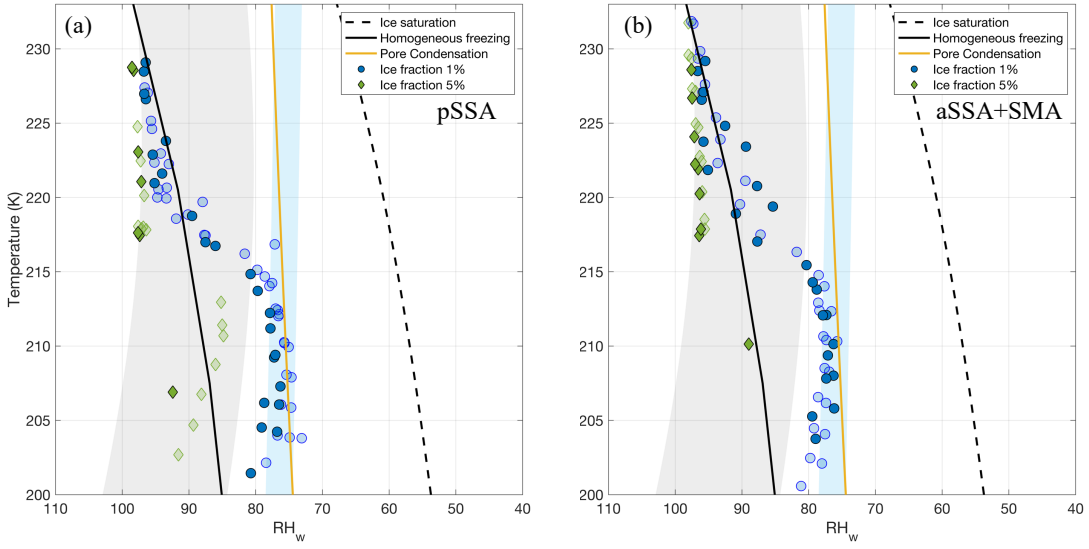

Figure 5. Fraction of frozen particles for (a) pSSA and (b) aSSA+SMA particles. The filled markers denote particles generated from the real seawater and the open markers from the artificial seawater. The blue and green markers indicate 1 %, and 5 % frozen fractions, respectively. The reference lines indicate ice saturation (black dashed), the parameterized RH_w for pore condensation in an 11 nm pore (Marcolli, 2014) (solid yellow), and the expected threshold for the onset of homogeneous freezing (Koop et al., 2000) (solid black). The blue shaded region represents the range of possible deliquescence RHs for NaCl and SSA, using the parameterization from Tang & Munkelwitz, (1993) for NaCl extrapolated to colder temperatures as the upper bound and shifting it down 4 % RH for SSA similar to Wagner et al., (2018). The gray shaded region represents the range of uncertainty for the homogeneous freezing parameterization for aqueous sulfuric acid particles as presented in Schneider et al. (2021b).

https://doi.org/10.5194/egusphere-2023-1016
Preprint. Discussion started: 14 June 2023

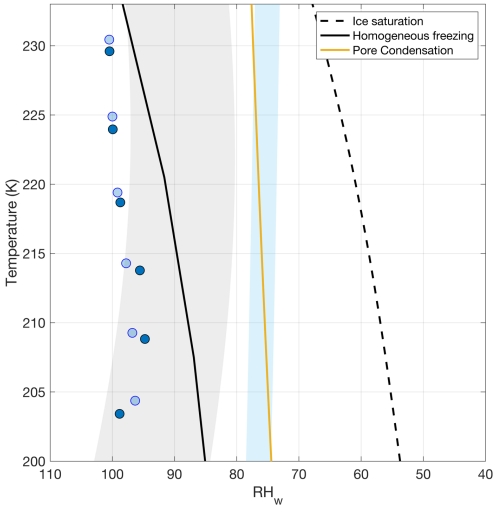

Figure 6. Similar to Figure 5, but only showing 1 % frozen fraction of SMA particles, where the filled and open markers denote SMA generated by sampling the headspace over real and artificial seawater, respectively.